ADVANCED FUNCTIONAL MATERIALS
www.afm-journal.de

Highly Efficient Greenish-Yellow Phosphorescent Organic Light-Emitting Diodes Based on Interzone Exciton Transfer

Yi-Lu Chang, Brett A. Kamino, Zhibin Wang, Michael G. Helander, Yingli Rao, Lily Chai, Suning Wang, Timothy P. Bender, and Zheng-Hong Lu**

Phosphorescent organic light emitting diodes (PHOLEDs) have undergone tremendous growth over the past two decades. Indeed, they are already prevalent in the form of mobile displays, and are expected to be used in large-area flat panels recently. To become a viable technology for next generation solid-state light source however, PHOLEDs face the challenge of achieving concurrently a high color rendering index (CRI) and a high efficiency at high luminance. To improve the CRI of a standard three color white PHOLED, one can use a greenish-yellow emitter to replace the green emitter such that the gap in emission wavelength between standard green and red emitters is eliminated. However, there are relatively few studies on greenish-yellow emitters for PHOLEDs, and as a result, the performance of greenish-yellow PHOLEDs is significantly inferior to those emitting in the three primary colors, which are driven strongly by the display industry. Herein, a newly synthesized greenish-yellow emitter is synthesized and a novel device concept is introduced featuring interzone exciton transfer to considerably enhance the device efficiency. In particular, high external quantum efficiencies (current efficiencies) of 21.5% (77.4 cd/A) and 20.2% (72.8 cd/A) at a luminance of 1000 cd/m^2 and 5000 cd/m^2, respectively, have been achieved. These efficiencies are the highest reported to date for greenish-yellow emitting PHOLEDs. A model for this unique design is also proposed. This design could potentially be applied to enhance the efficiency of even longer wavelength yellow and red emitters, thereby paving the way for a new avenue of tandem white PHOLEDs for solid-state lighting.

1. Introduction

Phosphorescent organic light emitting diodes (PHOLEDs) have undergone tremendous development[1–14] over the last two decades. Indeed, they are already prevalent in the form of mobile displays, and even are expected to be used in large-area flat panels recently. In order to become a viable technology for next generation solid-state light source however, PHOLEDs face the challenge of achieving simultaneously a high color rendering index (CRI) and a high efficiency at high luminance.[15,16] To improve the CRI, several groups have incorporated four or more emitters in order to cover the entire range of the visible spectrum.[17–20] However, the use of such high number of emitters not only increases device complexity, but also makes it less straightforward to achieve high device efficiency.[17–20] A more convenient approach to improve the CRI of a standard three color white (i.e. blue, green and red combination) PHOLED without sacrificing the overall device simplicity is to employ a greenish-yellow emitter to replace the green emitter such that the gap in emission wavelength between standard green and red emitters is eliminated.[21,22]

Unfortunately, there are relatively few reports on greenish-yellow emitters for PHOLEDs.[22–29] As a result, the performance of greenish-yellow emitters is significantly behind those emitting in the three primary colors, which are driven by the display industry. Hudson et al.[26,27] demonstrated a triarylboron-functionalized Pt(II) complex greenish-yellow emitter with a peak emission at 538 nm, that exhibits device external quantum efficiency (EQE) of 16.5%, current efficiency (CE) of 53.0 cd/A, and power efficiency (PE) of 45.0 lm/W at 1000 cd/m^2. So et al.[28] synthesized a trimethylsilylxylene-based greenish-yellow Ir(III) emitter with a peak wavelength at 532 nm, and demonstrated PHOLEDs with maximum EQE and CE of 12.7% and 45.7 cd/A, respectively, at ~10 cd/m^2. More recently, Chen et al.[22] reported a yellowish-green Ir(III) emitter with a peak wavelength at 544 nm, which exhibits a high CE of 63.0 cd/A at a luminance of 100 cd/m^2, corresponding to an EQE of 16.3% and power efficiency of 36.6 lm/W.

In this work, we demonstrate a newly synthesized greenish-yellow emitter that exhibits a decent EQE (CE) of ~15.2% (53.6 cd/A) at a luminance of 1000 cd/m^2. By introducing a novel design concept utilizing interzone exciton transfer, i.e., molecular energy transfer between adjacent emitting layers, we have significantly improved the device performance to a remarkable

Y.-L. Chang, Dr. Z. Wang, Dr. M. G. Helander, L. Chai, Prof. Z.-H. Lu
Department of Materials Science and Engineering
University of Toronto
184 College St., Toronto, Ontario, M5S 3E4, Canada
E-mail: yilu.chang@mail.utoronto.ca; zhenghong.lu@utoronto.ca
B. A. Kamino, Prof. T. P. Bender
Department of Chemical Engineering and Applied Chemistry
University of Toronto
200 College St., Toronto, Ontario, M5S 3E5, Canada
Y. Rao, Prof. S. Wang
Department of Chemistry
Queen's University
Kingston, Ontario, K7L 3N6, Canada

DOI: 10.1002/adfm.201202944

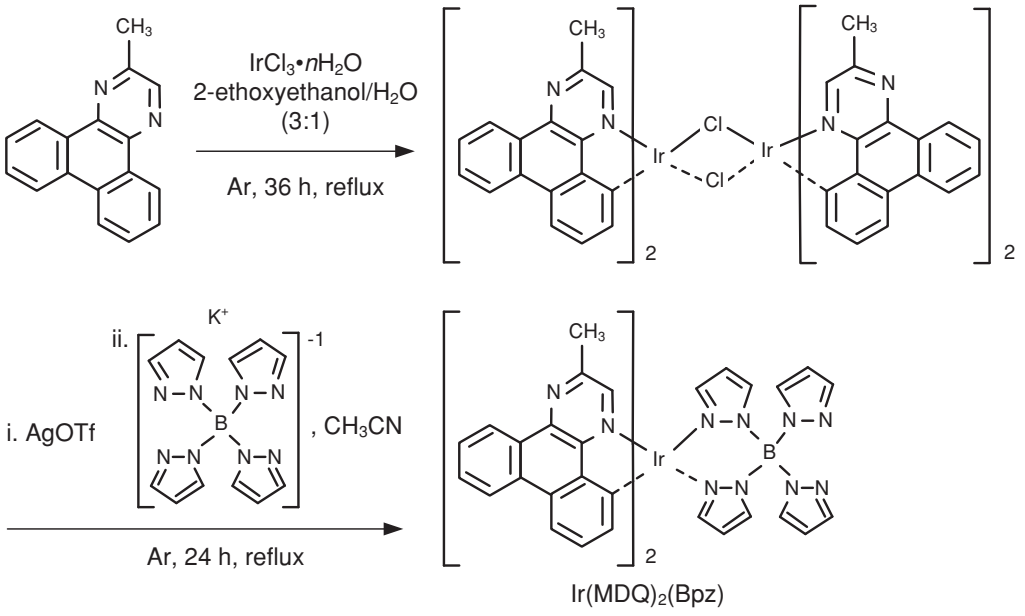

Scheme 1. Synthesis and structure of the greenish-yellow dopant used in this study.

EQE (CE) of 21.5% (77.4 cd/A) at 1000 cd/m^2. Even at a high luminance of 5000 cd/m^2 required for solid-state lighting, the EQE (CE) remains as high as 20.2% (72.8 cd/A). Such performance is comparable to that of the state-of-the-art green emitter, Ir(ppy)$_3$ [tris(2-phenylpyidine) iridium(III)],[30] and is the highest reported to date among greenish-yellow emitting PHOLEDs.

2. Results and Discussion

2.1. Molecular Design and Performance Characterization of Ir(MDQ)$_2$(Bpz)

It has been well-established that upon photoexcitation of an Ir-based metal-organic complex, two main electronic transitions will arise: 1) metal-to-ligand charge-transfer (MLCT) transition, where an electron is promoted from a metal *d* orbital to a vacant π^* orbital on one of the ligands, and 2) ligand-centered (LC) transition, where an electron is promoted between π orbitals on one of the coordinated ligands.[31,32] More importantly, due to the strong spin-orbit coupling exerted by the Ir metal core, triplet MLCT and LC transitions become dominant, yielding a total of four electronic states, i.e., singlet ^{1}MLCT and ^{1}LC as well as triplet ^{3}MLCT and ^{3}LC transition states.[31,32] The lowest excited state or the highly emissive state is generally consisted of an admixture (or a linear combination) of the lowest triplet states, ^{3}MLCT and ^{3}LC, or also known as a hybrid triplet state, T_1.[31–33] In order to tune the emission wavelength of the complex, substantial work has been carried out to alter the LC transition state energy by changing the ligand structure such as the incorporation of an electron-donating or electron-withdrawing substituent.[22,34–37] This change in ligand structure can effectively change the frontier orbital energies, thereby shifting the lowest unoccupied molecular orbital (LUMO) level that is localized on the cyclometalating ligands, and hence tuning the triplet state energy, T_1. Alternatively, one can also tune T_1 by changing the highest occupied molecular orbital (HOMO) level through the incorporation of various ancillary ligands that can affect the MLCT transition state energy.[38–40] Herein, in order to achieve a greenish-yellow emission, we have adopted the latter approach and successfully employed a well-known ancillary ligand, Bpz [tetrakis(1-pyrazolyl)-borate],[41] to modify a highly efficient, standard red phosphorescent emitter, Ir(MDQ)$_2$(acac) [bis(2-methyldibenzo[f,h]quinoxaline) (acetylacetonate) iridium(III)],[42] as schematically depicted in **Scheme 1**. The ancillary ligand Bpz is known previously for its remarkable blue-shifting capability by reducing the HOMO level of the Ir-complex that also led to a very high efficiency deep-blue emitter, Fir6 [bis(4,6-difluorophenylpyridinato) tetrakis(1-pyrazolyl)-borate iridium(III)].[39,43,44]

This newly synthesized molecule, Ir(MDQ)$_2$(Bpz) [bis(2-methyldibenzo[f,h]quinoxaline) tetrakis(1-pyrazolyl)-borate iridium(III)], exhibits a peak emission at ~539 nm that is ~70 nm blue-shifted compared to that of Ir(MDQ)$_2$(acac) as shown in **Figure 1**b. The Commission Internationale de l'Eclairage (CIE) coordinate of Ir(MDQ)$_2$(Bpz) is (0.378, 0.602), which corresponds to a greenish-yellow (GY) emission. Moreover, a decent absolute quantum yield[45] of ~0.74 is obtained for the GY emitter, which is slightly lower than that of the red emitter (R), Ir(MDQ)$_2$(acac), at ~0.77. This can be attributed to an increase in the MLCT transition energy or a reduction in the mixing of the ^{3}MLCT character into the lowest excited state, T_1, which resulted in a widening of the emission energy, following a decrease in the HOMO energy.[39] By conducting time-dependent density functional theory (TD-DFT) calculations,

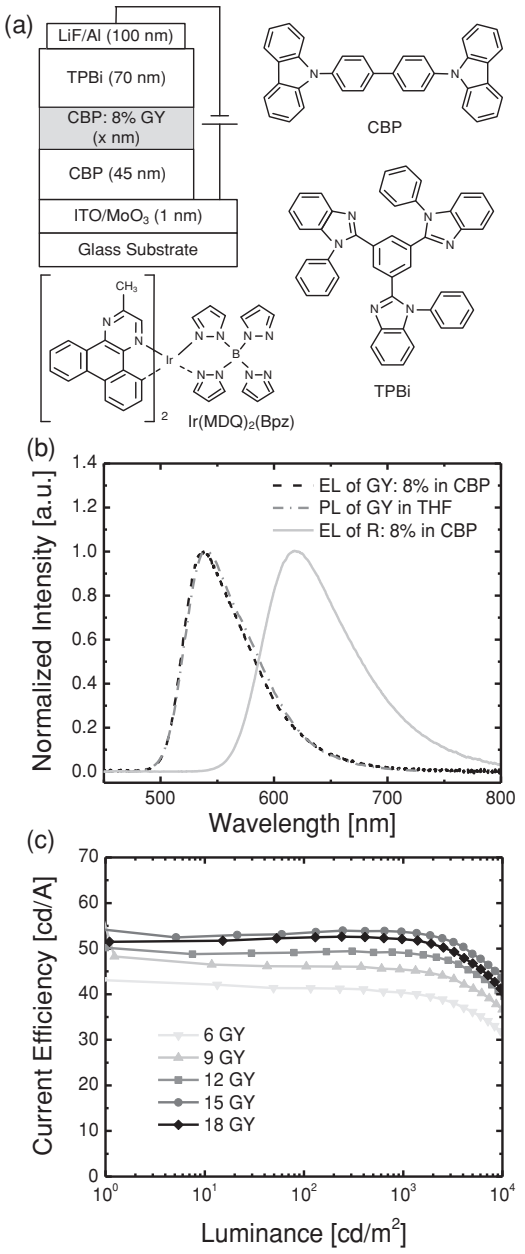

Figure 1. a) Device configuration and molecular structures of the materials used, where $Ir(MDQ)_2(Bpz)$ is used as the greenish-yellow (GY) emitter. All doping concentrations are in weight percentage. (b) Normalized EL spectra of GY-only and red (R)-only [$Ir(MDQ)_2(acac)$] devices as well as a normalized photoluminescence (PL) spectrum of the GY emitter in tetrahydrofuran (THF) (~ 1×10^{-5} M). (c) CE-L plot for the GY-only devices where the numbers shown in the legends represent the thickness (in nm) of the device emissive layer. A CE versus current density (CE-J) plot is also shown in Supporting Information Figure S2.

a geometry optimized structure with predicted HOMO and LUMO distributions for $Ir(MDQ)_2(Bpz)$ is illustrated in Supporting Information Figure S1.

To exploit the GY emitter in a device, we have implemented it in a simple, yet highly effective device architecture[46] as shown in Figure 1a. In this design, TPBi [2,2′,2″-(1,3,5-benzinetriyl)-tris(1-phenyl-1-H-benzimidazole)] is utilized as the electron transport layer (ETL) and CBP [4,4′-bis(carbazol-9-yl)biphenyl] is employed as both the hole transport layer (HTL) and the host material. The emissive layer consists of GY phosphor incorporated with varying thicknesses in host CBP starting from the CBP/TPBi interface. Standard ITO/MoO_3 anode and LiF/Al cathode are applied. In this design, the majority of the excitons will naturally generate near the HTL and ETL interface (i.e. the CBP/TPBi interface) on both sides, and are subsequently harvested (i.e. recombination takes place) on the doped regions of CBP by the GY emitter. After performance optimization as shown in Figure 1c, we have achieved a decent CE (EQE) of ~53.6 cd/A (15.2%) at a luminance of 1,000 cd/m^2 with a emissive layer thickness of 15 nm and a GY doping level of 8% in CBP, which is among the best greenish-yellow PHOLED performances reported to date.[22,26–28]

2.2. Efficiency Enhancement by Interzone Exciton Transfer

In order to further improve on the device performance, we have employed a novel design concept based on interzone exciton transfer as shown in **Figure 2**. This design involves the

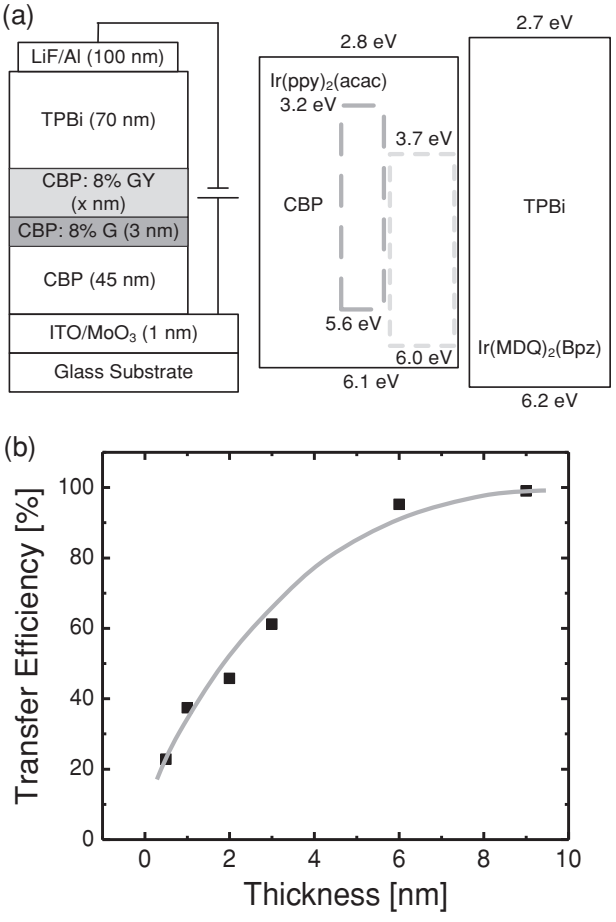

Figure 2. a) Device configuration based on interzone exciton transfer with a green (G) emissive layer incorporated, and the corresponding energy level diagram with respect to the vacuum level of all molecules considered. (b) Calculated energy transfer efficiency from G to greenish-yellow (GY) emitter versus the thickness of the GY emission layer.

incorporation of an additional thin layer (3 nm) of doped CBP using a green phosphor (G), $Ir(ppy)_2(acac)$ [bis(2-phenylpyridine)(acetylacetonate) iridium(III)], which is well-known for not only its high emission efficiency,[46,47] but also for its excellent exciton trapping capability in CBP.[36,48] In this configuration, the majority of the excitons formed near the CBP/TPBi interface will be harvested first by the GY emitter before the G emitter that is located farther away with respect to the HTL/ETL interface. More importantly, we expect that the higher energy G emitter will naturally transfer its energy to the adjacent lower energy GY emitter. Since the extent of such interzone exciton transfer is generally accepted to be ~3 nm,[4,5] our choice of the G emission zone thickness should in principle allow for a nearly complete energy transfer to the GY emission zone provided enough GY emissive sites are available.

The normalized electroluminescence (EL) spectra of the devices are shown in **Figure 3**. It is seen from Figure 3a that with an increase in thickness of the GY emitting layer, the spectra progressively red shift as more contribution from the GY emitter is present. Eventually, beyond a GY emitting layer thickness of 6 nm, the EL spectra becomes constant with a peak emission at 539 nm regardless of the presence of the G emitting layer as shown in Figure 3b. This suggests the GY emission layer has reached a thickness with sufficient GY emissive sites available to receive the majority of the excitons delivered from the G emitter. As the amount of GY emissive sites directly determines the energy transferred from the G emitter, the transfer efficiency will be directly proportional to the contribution of the GY emission in these GY + G devices. Using fits from the contribution of the individual EL spectra of the two emitters, we can quantitatively approximate the energy transfer efficiency from the G to GY emitter as shown in Figure 2b. It is apparent that a 6 nm thick layer of GY exhibits over 95% transfer efficiency and 9 nm demonstrates nearly perfect transfer of over 99%. Such efficient exciton energy transfer is further supported by a substantial overlap between the photoluminescence (PL) emission spectrum of the G emitter and the triplet ^{3}MLCT and ^{3}LC absorption states of the GY emitter as shown in Figure 3c. Interestingly, the fact that it required 6 nm to observe nearly complete energy transfer further suggests that the extent of such energy transfer could be substantially longer than the generally accepted value of ~3 nm, which has significant implications for the thickness of interlayer (nondoped host layer) required for the prevention of such interzone exciton transfer.[4,5] This long energy transfer range further suggests a Förster-type[49] mechanism is in place, either governed by angular momentum conservation[50] or facilitated by spin-orbit coupling.[51]

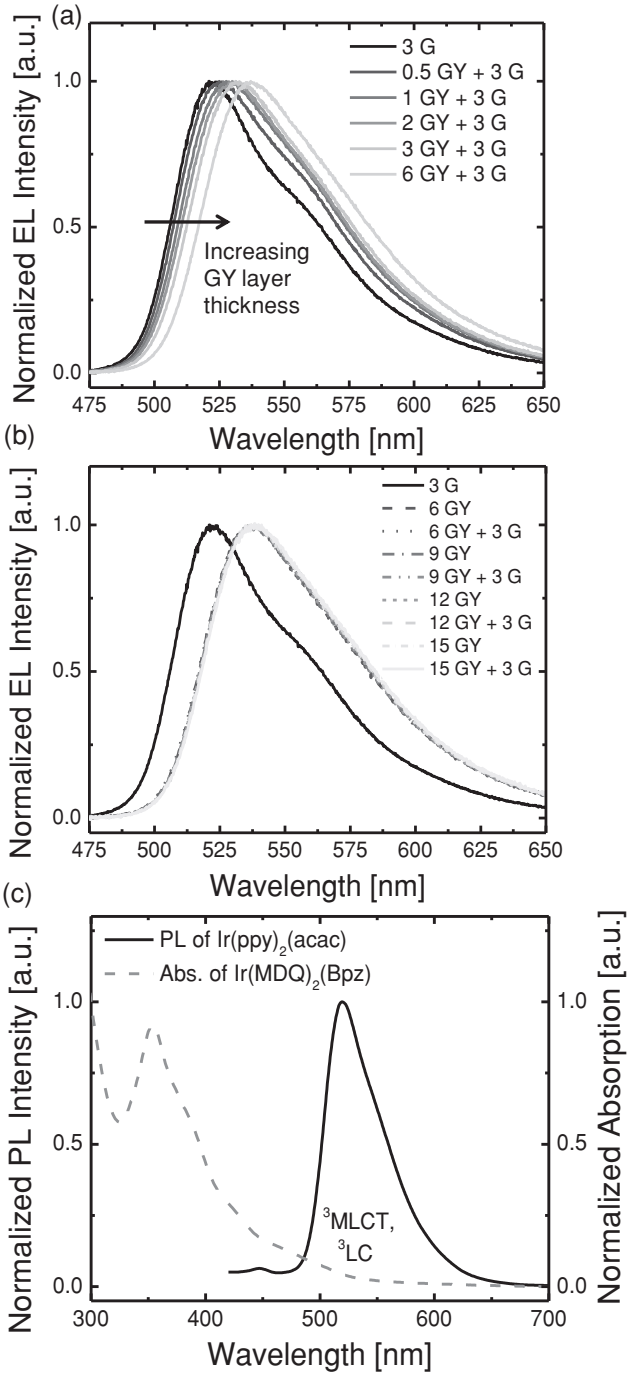

Figure 3. a,b) Normalized EL spectra of the GY + G devices considered. The numbers shown in the legends represent the thickness (in nm) of the device emission layer as depicted in Figure 2a. c) Solid-state PL spectrum of $Ir(ppy)_2(acac)$ doped in 50 nm thick CBP film and solution absorption spectrum of $Ir(MDQ)_2(Bpz)$ dissolved in CH_2Cl_2 (~1×10^{-5} M).

Figure 4 illustrates the performance characterization for devices with GY emission layer thickness of over 6 nm. It is seen from Figure 4a that with the G emission layer incorporation, the Current Efficiency versus Luminance (CE-L) plots are characterized by a dramatic increase in efficiency with luminance. This suggests that with increasing current density, more excitons formed in the host are able to reach the G emissive layer to be harvested, and subsequently transferred to the GY emissive sites efficiently. Remarkably, the optimum device with G emission layer incorporation (9 nm GY + 3 nm G) reaches a record high CE of 77.4 cd/A, which is ~1.4 times higher than the optimum device without the G emission layer at 53.6 cd/A at 1000 cd/m^2 as shown in Figure 4a. This also corresponds to an unprecedented EQE of 21.5% (see Figure 4b) for greenish-yellow emitting PHOLEDs reported to date. Even at a high luminance of 5000 cd/m^2 that is required for solid-state lighting, the

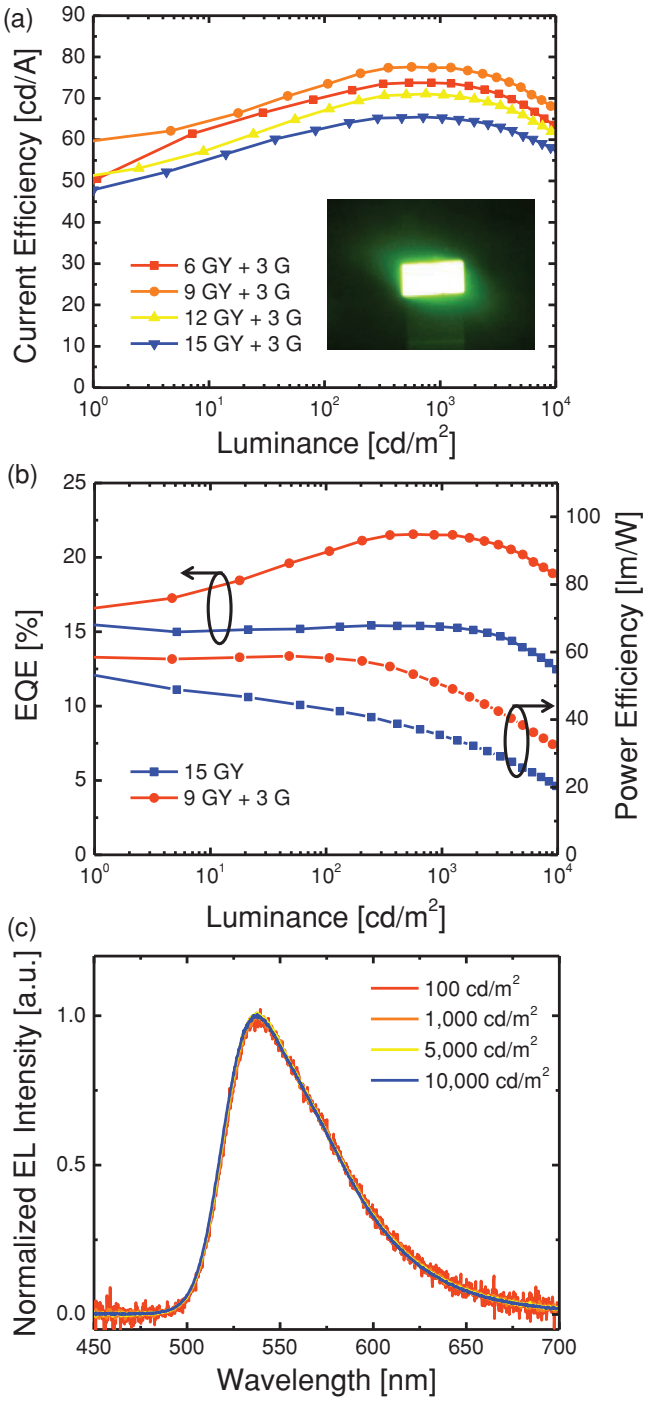

Figure 4. a) CE-L plots of the GY + G devices considered, with numbers in the legends denoting the thickness (in nm) of the device emissive layer. A photo of the optimized device (9 nm GY + 3 nm G) with an active area of 1 mm × 2 mm illuminating at 5,000 cd/m^2 is shown in the inset. A CE-J plot is also shown in Supporting Information Figure S3. b) EQE-PE-L plots of the optimized GY-only and GY + G devices. c) Normalized EL spectra of the optimized GY + G device (9 nm GY + 3 nm G) at a wide range of luminance levels.

EQE (CE) remains as high as 20.2% (72.8 cd/A). The enhancement in power efficiency (PE) is also impressive as shown in Figure 4b. A high PE of 50.7 lm/W is achieved at 1000 cd/m^2, which is considerably higher than that of the optimum device without G emission layer at 34.9 lm/W. Furthermore, Figure 4c shows extremely stable EL spectra under varying luminance (or current density), which indicates that excitons are well-confined in the emissive zones in our design owning to the high triplet energy levels of both CBP and TPBi.[7] The stable spectra also suggest that the energy transfer from the G to the GY emitter remains proficient under a wide range of current injection levels. It is worth noting that beyond a GY layer thickness of 9 nm, the device performance reaches saturation presumably due to increased charge imbalance or reduced optical out-coupling in the device given the increased total device thickness.

Although efficient energy transfer from the G to GY emission layer is established, this alone could not fully explain the significant performance improvement in our devices. We therefore further characterize the devices by examining the spectral power (total radiant power per wavelength) of the optimized device with and without G emission layer under a fixed current density as shown in **Figure 5**. It is observed that the enhancement

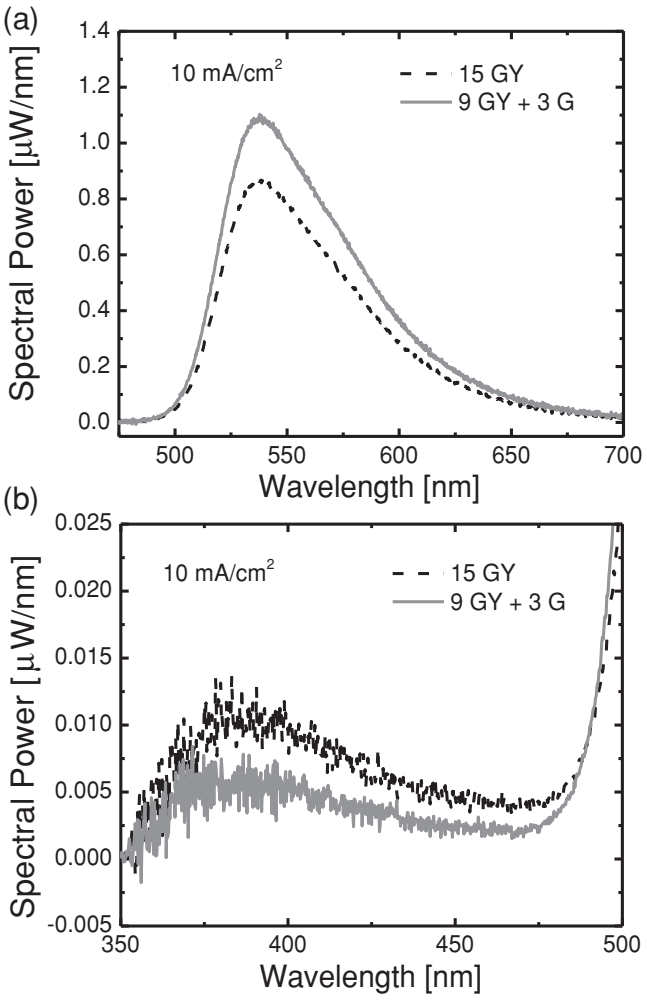

Figure 5. Spectral power spectra of the optimized GY-only and GY + G devices at a) long and b) short wavelength ranges. A considerably higher host emission is observed for the optimized GY-only device. The numbers shown in the legends stand for the thickness (in nm) of the device emissive layers.

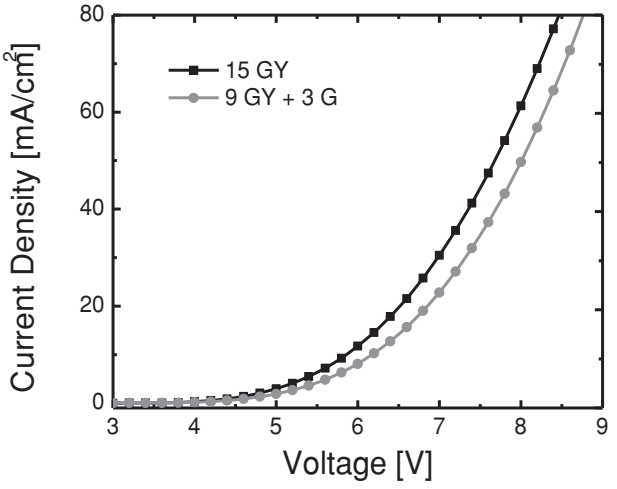

Figure 6. Current density versus voltage (*J–V*) plot of the optimized GY-only and GY + G devices. A lower current density is seen for the GY + G device, suggesting more carrier trapping is present. The numbers shown in the legends indicate the thickness (in nm) of the device emissive layers.

in spectral intensity with G emission layer is consistent with the device efficiency enhancement. More importantly, from Figure 5b we note a considerably reduced host emission from the device with G emission layer incorporation. This suggests that the G emission layer is able to further utilize the excitons that would have otherwise been wasted by the GY emission layer. Additionally, from the energy level diagram in Figure 2a, we observe a considerably higher HOMO level for the G emitter at 5.6 eV as compared to those of the host CBP (6.1 eV) and the GY emitter (6.0 eV), which suggests an improved hole trapping by the G emitter in CBP, and hence direct exciton formation on the G emitter is highly probable. This carrier trapping phenomenon is also evidenced by the lower current density of the device with G layer incorporation as shown in **Figure 6**. We can therefore understand that the G emitter is not only capable of directly forming excitons, but also further harnessing excitons in the host that are unused by or leaked through the GY emission layer, and subsequently perform efficient exciton transfer to the adjacent GY emissive sites, thereby significantly enhancing the efficiency of the overall device.

The above mechanism can be modeled as follows:

$$\eta_{ext} = \gamma \eta_{oc} \eta_{E-P} \tag{1a}$$

$$= \gamma \eta_{oc} \chi \phi_{PL} \tag{1b}$$

$$= \gamma \eta_{oc} \{ i_{GY} \chi_{GY} \phi_{PL,GY} + i_G \chi_G [\eta_{G-GY} \phi_{PL,GY} + (1-\eta_{G-GY}) \phi_{PL,G}] \} \tag{1c}$$

where η_{ext}, η_{oc}, $\eta_{E\text{-}P}$ and $\eta_{G\text{-}GY}$ represent device external quantum efficiency, out-coupling efficiency, exciton-to-photon conversion efficiency and energy transfer efficiency from G to GY emitter, respectively. γ, $\phi_{PL,}$ *and* χ denote charge balance factor, absolute quantum yield of each emitter, and fraction of emissive excitons trapped by each emitter in the device, respectively. We further define i as the ideality factor accounting for the reduction in the fraction of emissive excitons trapped by each emitter with an emissive layer thickness that deviates from the optimum thickness. From Equation (1c), it is apparent that a high fraction of emissive excitons trapped by the G emitter, χ_G, together with high energy transfer efficiency from G to GY emitters, $\eta_{G\text{-}GY}$, can significantly enhance the overall device efficiency with a predominant GY emission. Using optimized device parameters for single-color G and GY devices (see Supporting Information), we can deduce the fraction of emissive excitons trapped in the device, χ_G and χ_{GY}, to be ~0.96 and ~0.71, respectively. By applying Equation 1c, a projected η_{ext} at 1000 cd/m^2 is found to be ~22%, which is in excellent agreement with that achieved from the optimal GY + G device shown in Figure 4b.

3. Conclusions

In summary, we have synthesized a carefully designed greenish-yellow emitter, Ir(MDQ)$_2$(Bpz), and introduced a novel device concept featuring interzone exciton transfer to considerably enhance the device efficiency. Specifically, an exciton harnessing green emissive layer is inserted in the device to minimize exciton leakage and subsequently transfer the excitons to the adjacent greenish-yellow emitter efficiently, thereby boosting the efficiency of the greenish-yellow emission. High EQEs (CEs) of 21.5% (77.4 cd/A) and 20.2% (72.8 cd/A) at a luminance of 1000 cd/m^2 and 5000 cd/m^2, respectively, have been achieved, which represent the highest performance reported to date among greenish-yellow emitting PHOLEDs. A model is further proposed to explain the exciton harnessing process in this new device architecture involving interzone exciton transfer. This design in principle could also be applied to enhance the efficiency of even longer wavelength yellow and red emitters, thereby paving the way for a new avenue of tandem or stacked[52–56] white PHOLEDs based on interzone exciton transfer. We anticipate that our design concept will significantly advance the development of high efficiency PHOLEDs for displays and solid-state lighting.

4. Experimental Section

Synthesis of Complex Ir(MDQ)$_2$(Bpz): Ligand 2-methyl-dibenzo[*f*,*h*] quinoxaline (MDQ) was first prepared according to the procedure reported in ref.[42]. MDQ (2.3 mmol) was then dissolved in 2-ethoxyethanol (10 mL) in a 50 mL flask. Subsequently, iridium trichloride hydrate (1.0 mm) and 3 mL of water were added into the flask. The mixture was stirred under argon for 36 h at 120 °C. The mixture was then allowed to cool to room temperature and the precipitate was collected and washed with acetone, ethanol, and dried in vacuum to yield a cyclometalated Ir^{III}-μ-chloro-bridged dimer. The dimer (1.0 mmol) was then dissolved in 25 mL of CH_2Cl_2 and mixed with AgOTf (2.2 mmol), which was separately dissolved in 25 mL of MeOH, and stirred under Ar for 2 h at room temperature. The mixture was then centrifuged at 5000 rpm for 10 min to separate out AgCl precipitate. The mixture was further evaporated to dryness. Next, potassium tetrakis(1-pyrazolyl)-borate salt was prepared according to the procedure reported in ref.[41]. The mixture was then dissolved in 25 mL of CH_3CN and treated with the salt (3.5 mmol) and refluxed under argon for 24 h. After cooling to room temperature, the precipitate was washed with CH_3CN and dissolved in CH_2Cl_2. A silica flash column using hexane and ethyl acetate solvent system was applied to yield the final pure product.

Ir(MDQ)$_2$(Bpz): Yield: 70%. ^{1}H NMR (400 MHz, $CDCl_3$): δ 9.24 (dd, J_1 = 8.0 Hz, J_2 = 1.6 Hz, 2H), 8.55 (d, J = 7.2 Hz, 2H), 8.02 (d, J = 8.2 Hz, 2H), 7.77 (m, 6H), 7.39 (s, 2H), 7.20 (d, J = 2.5 Hz, 2H), 7.12 (t, J = 7.7 Hz, 2H), 7.00 (d, J = 1.9 Hz, 2H), 6.18 (m, 6H), 6.02 (t, J = 1.9 Hz, 2H), 2.77 (s, 6H). ^{13}C NMR (100 MHz, $CDCl_3$): δ 153.7, 149.7, 146.9, 144.8, 142.4(8), 142.4(6), 142.1, 141.9, 139.0, 138.8, 133.7, 133.0, 131.4, 130.0, 129.2, 129.1, 127.45, 125.3, 123.3, 115.7, 107.0, 105.4. Full proton and carbon spectra are shown in Supporting Information Figures S4 and S5, respectively. HRMS (Dart) calc'd for $C_{46}H_{35}BN_{12}Ir$ $[M+H]^+$: 959.2824, found 959.2810. Anal. calc'd for $C_{46}H_{34}BN_{12}Ir$: C 57.68, H 3.58, N 17.55, found: C 57.49, H 3.51, N 17.37.

Device Fabrication and Characterization: All PHOLEDs were fabricated via thermal evaporation using a Kurt J. Lesker LUMINOS cluster tool at a base pressure of ~10^{-8} Torr. The substrate used consists of glass (1.1 mm thick) that is pre-coated with indium tin oxide (ITO), with a thickness and sheet resistance of 120 nm and 15 Ω/sq, respectively. Before loading, the substrate was degreased using standard solvents, blow-dried using a N_2 gun, and treated in a UV-ozone chamber for 10 min. All doping concentration used in this work are by weight percentage. The active area for each device was ~2 mm^2 as confirmed with an optical microscope before device characterization. The deposited layer thickness was monitored by a quartz crystal microbalance which was calibrated by spectroscopic ellipsometry (Sopra GES 5E). All dopants used were purified by gradient sublimation prior to usage to ensure the highest purity attainable. An accurate control of layer thicknesses during the device fabrication and a high purity of the phosphorescent emitters were found to be critical to achieve highly efficient devices with high reproducibility. Luminance-Voltage measurements were performed using a Minolta LS-110 Luminance Meter. Current–Voltage characteristics were obtained using an HP4140B pA meter. The radiant flux for calculating EQEs was measured using an integrating sphere equipped with an Ocean Optics USB 4000 spectrometer with NIST traceable calibration using a halogen lamp.[57]

PL measurements: The solution PL measurements were carried out using Perkin Elmer LS55 fluorescence spectrometer and the absorption measurements were performed using Perkin Elmer Lambda 25 UV-vis spectrometer. The absolute quantum yield measurements were performed using a custom built setup according to the procedure reported in ref.[45]. A 365 nm collimated LED from Thorlabs (M365L2-C2) was used as the excitation source, which was directed onto the sample consisted of a doped organic film (100 nm thick of phosphor-doped CBP) deposited on a quartz substrate (1 mm thick) and mounted inside a calibrated integrating sphere. The light generated was then detected using an Ocean Optics Maya 2000 Pro spectrometer.

TD-DFT Calculations: Molecular orbital and molecular geometry calculations were performed using the Gaussian 03 program suite with crystal structures as the starting point for geometry optimizations where possible. Calculations were performed at the B3LYP level of theory by using LAN2LDZ as the basis set for Ir, and 6-31G* for all other atoms.

Supporting Information

Supporting Information is available from the Wiley Online Library or from the author

Acknowledgements

The authors would like to acknowledge funding for this research from the Natural Sciences and Engineering Research Council (NSERC) of Canada. Z.H.L. is a Government of Canada Research Chair in Organic Optoelectronics; Tier I.

Received: October 10, 2012
Revised: December 11, 2012
Published online: January 30, 2013

[1] G. J. Zhou, W. Y. Wong, S. Suo, *J. Photochem. Photobiol., C* **2010**, *11*, 133.
[2] G. J. Zhou, W. Y. Wong, X. L. Yang, *Chem.-Asian J.* **2011**, *6*, 1706.
[3] S. Lamansky, P. Djurovich, D. Murphy, F. Abdel-Razzaq, H. E. Lee, C. Adachi, P. E. Burrows, S. R. Forrest, M. E. Thompson, *J. Am. Chem. Soc.* **2001**, *123*, 4304.
[4] Y. R. Sun, N. C. Giebink, H. Kanno, B. W. Ma, M. E. Thompson, S. R. Forrest, *Nature* **2006**, *440*, 908.
[5] S. Reineke, F. Lindner, G. Schwartz, N. Seidler, K. Walzer, B. Lussem, K. Leo, *Nature* **2009**, *459*, 234.
[6] J. Ye, C. J. Zheng, X. M. Ou, X. H. Zhang, M. K. Fung, C. S. Lee, *Adv. Mater.* **2012**, *24*, 3410.
[7] L. X. Xiao, Z. J. Chen, B. Qu, J. X. Luo, S. Kong, Q. H. Gong, J. J. Kido, *Adv. Mater.* **2011**, *23*, 926.
[8] B. H. Zhang, G. P. Tan, C. S. Lam, B. Yao, C. L. Ho, L. H. Liu, Z. Y. Xie, W. Y. Wong, J. Q. Ding, L. X. Wang, *Adv. Mater.* **2012**, *24*, 1873.
[9] H. Sasabe, J. Takamatsu, T. Motoyama, S. Watanabe, G. Wagenblast, N. Langer, O. Molt, E. Fuchs, C. Lennartz, J. Kido, *Adv. Mater.* **2010**, *22*, 5003.
[10] S. J. Su, E. Gonmori, H. Sasabe, J. Kido, *Adv. Mater.* **2008**, *20*, 4189.
[11] Q. Wang, J. Q. Ding, D. G. Ma, Y. X. Cheng, L. X. Wang, F. S. Wang, *Adv. Mater.* **2009**, *21*, 2944.
[12] M. A. Baldo, D. F. O'Brien, Y. You, A. Shoustikov, S. Sibley, M. E. Thompson, S. R. Forrest, *Nature* **1998**, *395*, 151.
[13] W. Y. Wong, C. L. Ho, *Coord. Chem. Rev.* **2009**, *253*, 1709.
[14] W. Y. Wong, C. L. Ho, *J. Mater. Chem.* **2009**, *19*, 4457.
[15] G. J. Zhou, Q. Wang, C. L. Ho, W. Y. Wong, D. G. Ma, L. X. Wang, *Chem. Commun.* **2009**, *24*, 3574.
[16] G. J. Zhou, Q. Wang, X. Z. Wang, C. L. Ho, W. Y. Wong, D. G. Ma, L. X. Wang, Z. Y. Lin, *J. Mater. Chem.* **2010**, *20*, 7472.
[17] J. H. Jou, Y. C. Chou, S. M. Shen, M. H. Wu, P. S. Wu, C. R. Lin, R. Z. Wu, S. H. Chen, M. K. Wei, C. W. Wang, *J. Mater. Chem.* **2011**, *21*, 18523.
[18] J. H. Jou, S. M. Shen, C. R. Lin, Y. S. Wang, Y. C. Chou, S. Z. Chen, Y. C. Jou, *Org. Electron.* **2011**, *12*, 865.
[19] Y. B. Zhao, J. S. Chen, D. G. Ma, *Appl. Phys. Lett.* **2011**, *99*, 163303.
[20] T. C. Rosenow, M. Furno, S. Reineke, S. Olthof, B. Lussem, K. Leo, *J. Appl. Phys.* **2010**, *108*, 113113.
[21] Y. S. Park, J. W. Kang, D. M. Kang, J. W. Park, Y. H. Kim, S. K. Kwon, J. J. Kim, *Adv. Mater.* **2008**, *20*, 1957.
[22] S. M. Chen, G. P. Tan, W. Y. Wong, H. S. Kwok, *Adv. Funct. Mater.* **2011**, *21*, 3785.
[23] G. J. Zhou, Q. Wang, W. Y. Wong, D. G. Ma, L. X. Wang, Z. Y. Lin, *J. Mater. Chem.* **2009**, *19*, 1872.
[24] C. L. Ho, Q. Wang, C. S. Lam, W. Y. Wong, D. G. Ma, L. X. Wang, Z. Q. Gao, C. H. Chen, K. W. Cheah, Z. Y. Lin, *Chem.-Asian J.* **2009**, *4*, 89.
[25] C. L. Ho, L. C. Chi, W. Y. Hung, W. J. Chen, Y. C. Lin, H. Wu, E. Mondal, G. J. Zhou, K. T. Wong, W. Y. Wong, *J. Mater. Chem.* **2012**, *22*, 215.
[26] Z. M. Hudson, C. Sun, M. G. Helander, H. Amarne, Z. H. Lu, S. N. Wang, *Adv. Funct. Mater.* **2010**, *20*, 3426.
[27] Z. B. Wang, M. G. Helander, Z. M. Hudson, J. Qiu, S. Wang, Z. H. Lu, *Appl. Phys. Lett.* **2011**, *98*, 213301.
[28] K. H. So, R. Kim, H. Park, I. Kang, K. Thangaraju, Y. S. Park, J. J. Kim, S. K. Kwon, Y. H. Kim, *Dyes Pigm.* **2012**, *92*, 603.
[29] G. J. Zhou, C. L. Ho, W. Y. Wong, Q. Wang, D. G. Ma, L. X. Wang, Z. Y. Lin, T. B. Marder, A. Beeby, *Adv. Funct. Mater.* **2008**, *18*, 499.
[30] S. Watanabe, N. Ide, J. Kido, *Jpn. J. Appl. Phys.* **2007**, *46*, 1186.
[31] A. Tsuboyama, H. Iwawaki, M. Furugori, T. Mukaide, J. Kamatani, S. Igawa, T. Moriyama, S. Miura, T. Takiguchi, S. Okada, M. Hoshino, K. Ueno, *J. Am. Chem. Soc.* **2003**, *125*, 12971.
[32] M. S. Lowry, S. Bernhard, *Chem.-Eur. J.* **2006**, *12*, 7970.
[33] Y. You, W. Nam, *Chem. Soc. Rev.* **2012**, *41*, 7061.

[34] W. C. Chang, A. T. Hu, J. P. Duan, D. K. Rayabarapu, C. H. Cheng, *J. Organomet. Chem.* **2004**, *689*, 4882.
[35] D. H. Kim, N. S. Cho, H. Y. Oh, J. H. Yang, W. S. Jeon, J. S. Park, M. C. Suh, F. H. Kwon, *Adv. Mater.* **2011**, *23*, 2721.
[36] R. J. Wang, D. Liu, H. C. Ren, T. Zhang, H. M. Yin, G. Y. Liu, J. Y. Li, *Adv. Mater.* **2011**, *23*, 2823.
[37] S. J. Yeh, M. F. Wu, C. T. Chen, Y. H. Song, Y. Chi, M. H. Ho, S. F. Hsu, C. H. Chen, *Adv. Mater.* **2005**, *17*, 285.
[38] M. K. Nazeeruddin, R. Humphry-Baker, D. Berner, S. Rivier, L. Zuppiroli, M. Graetzel, *J. Am. Chem. Soc.* **2003**, *125*, 8790.
[39] J. Li, P. I. Djurovich, B. D. Alleyne, M. Yousufuddin, N. N. Ho, J. C. Thomas, J. C. Peters, R. Bau, M. E. Thompson, *Inorg. Chem.* **2005**, *44*, 1713.
[40] L. Q. Chen, C. L. Yang, J. G. Qin, J. Gao, H. You, D. G. Ma, *J. Organomet. Chem.* **2006**, *691*, 3519.
[41] J. Li, P. I. Djurovich, B. D. Alleyne, I. Tsyba, N. N. Ho, R. Bau, M. E. Thompson, *Polyhedron* **2004**, *23*, 419.
[42] J. P. Duan, P. P. Sun, C. H. Cheng, *Adv. Mater.* **2003**, *15*, 224.
[43] R. J. Holmes, B. W. D'Andrade, S. R. Forrest, X. Ren, J. Li, M. E. Thompson, *Appl. Phys. Lett.* **2003**, *83*, 3818.
[44] B. W. D'Andrade, R. J. Holmes, S. R. Forrest, *Adv. Mater.* **2004**, *16*, 624.
[45] Y. Kawamura, H. Sasabe, C. Adachi, *Jpn. J. Appl. Phys.* **2004**, *43*, 7729.
[46] Z. B. Wang, M. G. Helander, J. Qiu, D. P. Puzzo, M. T. Greiner, Z. W. Liu, Z. H. Lu, *Appl. Phys. Lett.* **2011**, *98*, 073310.
[47] C. Adachi, M. A. Baldo, M. E. Thompson, S. R. Forrest, *J. Appl. Phys.* **2001**, *90*, 5048.
[48] Y.-L. Chang, Z. B. Wang, M. G. Helander, J. Qiu, D. P. Puzzo, Z. H. Lu, *Org. Electron.* **2012**, *13*, 925.
[49] T. Forster, *Discuss. Faraday Soc.* **1959**, *27*, 7.
[50] D. Guo, T. E. Knight, J. K. McCusker, *Science* **2011**, *334*, 1684.
[51] G. D. Scholes, *Annu. Rev. Phys. Chem.* **2003**, *54*, 57.
[52] J. Sun, X. L. Zhu, H. J. Peng, M. Wong, H. S. Kwok, *Org. Electron.* **2007**, *8*, 305.
[53] T. W. Lee, T. Noh, B. K. Choi, M. S. Kim, D. W. Shin, J. Kido, *Appl. Phys. Lett.* **2008**, *92*, 043301.
[54] H. Kanno, N. C. Giebink, Y. R. Sun, S. R. Forrest, *Appl. Phys. Lett.* **2006**, *89*, 023503.
[55] H. Kanno, R. J. Holmes, Y. Sun, S. Kena-Cohen, S. R. Forrest, *Adv. Mater.* **2006**, *18*, 339.
[56] Q. Wang, J. Q. Ding, Z. Q. Zhang, D. G. Ma, Y. X. Cheng, L. X. Wang, F. S. Wang, *J. Appl. Phys.* **2009**, *105*, 076101.
[57] S. R. Forrest, D. D. C. Bradley, M. E. Thompson, *Adv. Mater.* **2003**, *15*, 1043.